JACS
JOURNAL OF THE AMERICAN CHEMICAL SOCIETY
pubs.acs.org/JACS
Article

Composition Determination of Heterometallic Trinuclear Clusters via Anomalous X-ray and Neutron Diffraction

Cristin E. Juda, Claire E. Casaday, Justin J. Teesdale, Amymarie K. Bartholomew, Benjamin Lin, Kurtis M. Carsch, Rebecca A. Musgrave, Shao-Liang Zheng, Xiaoping Wang, Christina M. Hoffmann, SuYin Wang, Yu Sheng Chen, and Theodore A. Betley*

Cite This: J. Am. Chem. Soc. 2024, 146, 30320−30331
Read Online
ACCESS | Metrics & More | Article Recommendations | Supporting Information

ABSTRACT: Anomalous X-ray diffraction (AXD) and neutron diffraction can be used to crystallographically distinguish between metals of similar electron density. Despite the use of AXD for structural characterization in mixed metal clusters, there are no benchmark studies evaluating the accuracy of AXD toward assessing elemental occupancy in molecules with comparisons with what is determined via neutron diffraction. We collected resonant diffraction data on several homo and heterometallic clusters and refined their anomalous scattering components to determine metal site occupancies. Theoretical resonant scattering terms for Fe^0, Co^0, and Zn^0 were compared against experimental values, revealing theoretical values are ill-suited to serve as references for occupancy determination. The cluster featuring distinct cation and anion metal compositions $[CoCp_2^*][(^{tbs}L)Fe_3(\mu^3{-}NAr)]$ was used to assess the accuracy of different f' references for occupancy determination ($f'_{theoretical}$ ± 15−17%; $f'_{experimental}$ ± 10%). This methodology was applied toward calculating the occupancy of three different clusters: $(^{tbs}L)Fe_2Zn(py)$ (**6**), $(^{tbs}L)Fe_2Zn(\mu^3{-}NAr)(py)$ (**7**), and $[CoCp^*_2][(^{tbs}L)Fe_2Zn(\mu^3{-}NAr)]$ (**8**). The first two clusters maintain 100% Fe/Zn site isolation, whereas **8** showed metal mixing within the sites. The large crystal size of **8** enabled collection of neutron diffraction data which was compared against the results found with AXD. The ability of AXD to replicate the metal occupancies as determined by neutron diffraction supports the AXD occupancy methodology developed herein. Furthermore, the advantages innate to AXD (e.g., smaller crystal sizes, shorter collection times, and greater availability of synchrotron resources) versus neutron diffraction further support the need for its development as a standard technique.

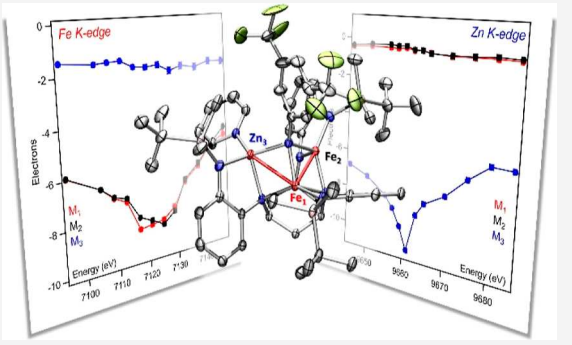

1. INTRODUCTION

Biological and synthetic catalysts often feature active sites with mixed-metal compositions allowing for the precise tuning of redox for small molecule activation.[1−4] Multinuclear heterometallic clusters are prone to metal-atom scrambling when closely sized metals are proximally oriented and have similar ligand environments.[5−11] A thorough understanding of the electronic structure of these catalysts depends on quantifying the substitutional homogeneity of each metal site, a difficult task with traditional crystallography.

Standard single crystal X-ray diffraction (SCXRD) is an invaluable tool for determining connectivity in paramagnetic clusters. Using traditional laboratory sources, however, SCXRD is limited in the information it can unambiguously provide for heteronuclear clusters. At high energy X-ray wavelengths, for example 17.445 keV (Mo Kα), transition metals nearby on the periodic table scatter radiation similarly.[12,13] The similar scattering of nearby metals convolutes distinguishing between different metals at one site within a heteronuclear cluster.

Two diffraction techniques are employed to gain information on metal atom identity within heterometallic materials: anomalous X-ray diffraction (AXD, also known as resonant diffraction) and neutron diffraction. AXD is a crystallographic phenomenon whereby large changes to atomic scattering factors occur at elemental absorption K-edges.[13−17] AXD has been used to solve the phase problem in macromolecular structures,[2,3,18−23,44] assign atomic distributions in heterometallic proteins,[24,40] materials,[25−36] and molecules,[37−39,41−43] determine metal oxidation level in monometallic[45] and multinuclear[46−56] molecules, improve the refinement of structures containing heavy atoms,[78,79] and probe chemical dynamics.[80] In contrast to atomic scattering factors, neutron scattering lengths do not display periodic trends.[57,58]

Received: July 26, 2024
Revised: October 10, 2024
Accepted: October 11, 2024
Published: October 26, 2024

Consequently, the neutron scattering lengths across the first-row transition metals vary greatly; for example, the neutron scattering length for Fe is 9.45 fm, while the scattering length for Zn is 5.68 fm (see Table 1).[58] Thus, probing metal sites in heterometallic species containing Fe and Zn with neutron diffraction results in a 50% difference in scattering as compared to the ∼15% difference with Mo Kα radiation. Due to this large difference, neutron diffraction has historically been applied to materials,[59−62] minerals,[63−65] extended networks,[31,33,66,67] and molecules[68,69] as a means of discerning metal identity in heterometallic structures.

Table 1. X-ray Anomalous Scattering Components and Neutron Scattering Factors for Fe and Zn

radiation	Fe		Zn	
source	f'	f''	f'	f''
Mo Kα (17.45 keV)	0.199	0.306	0.260	0.537
synchrotron (30 keV)	0.346	0.844	0.2839	1.4301
Fe K-edge (7.1 keV)	−5.96	1.28	−2.65	2.55
Zn K-edge (9.65 keV)	−0.22	2.56	−7.24	1.55
neutron	9.45 fm		5.68 fm	

The present study seeks to evaluate the accuracy of AXD structure factors for characterizing metal atom substitution within heterometallic clusters and outline a systematic approach for applying this technique to molecules. Occupancy determination at each metal site using AXD relies on comparing theoretical anomalous scattering components to experimental scattering perturbations (f' and f''). However, determining whether differences between experimental and theoretical values are due to mixed occupancy at the site or other factors can be difficult. To address this difficulty, we evaluate the anomalous scattering components of metal ions in homometallic standards and compare them to theoretically predicted values. Next, we evaluate the accuracy of several reference f' values at predicting f' in molecular environments. These findings are then applied toward determining the occupancy of previously reported [Fe_2Zn] heterometallic clusters. Finally, the AXD results on a mixed metal [Fe_2Zn] cluster which experiences site-mixing are compared against results obtained via neutron diffraction. The work presented herein serves to (1) establish the intrinsic error of AXD occupancy studies; (2) provide a benchmark for future AXD occupancy studies on heterometallic molecules; and (3) directly compare the results of AXD and neutron diffraction occupancy studies.

2. EXPERIMENTAL BACKGROUND AND DESIGN

2.1. Anomalous X-ray Diffraction: Theoretical Background. The physical basis of X-ray diffraction stems from the scattering of incident radiation by electrons. In the classical description of scattering, electrons residing in atoms are treated as dipoles oscillating in an electromagnetic field. The electron oscillates with the same frequency of the incident radiation, and the amplitude of that motion is described by the following equation

$$A = \frac{e}{m}\cdot\frac{E_0}{\omega_0^2 - \omega^2 + ik\omega} \tag{1}$$

where e is the charge of an electron, m is the mass of the electron, E_0 is the electric field amplitude, ω is the frequency of the incident radiation, ω_0 is the natural oscillation frequency of an electron, and k is the Hooke's law constant.[12−14] The atomic scattering factor (f) is defined by the ratio of the atom's scattering amplitude (A) to the scattering amplitude of a free electron defined in the classical limit (Thomson scattering).[12] Because electrons exist in atomic orbitals which resonate at characteristic frequencies, this description of scattering falls short as ω tends toward ω_0, the resonant frequency of an electron. As the X-ray oscillatory frequency approaches an atomic orbital frequency, the induced electronic vibrations resonate at the natural oscillations of the bound electrons, i.e. those corresponding to electronic transitions. These scattering perturbations add to the "normal" scattering (f_0) and are referred to as anomalous scattering components (or dispersion correction factors).[15−17]

$$f = f_0 + f' + if'' \tag{2}$$

$$\text{where } f'(\omega) = \frac{\omega^2(\omega^2 - \omega_o^2)}{(\omega^2 - \omega_o^2)^2 + k^2\omega^2} \tag{2.1}$$

$$\text{and } f''(\omega) = \frac{k\omega^3}{(\omega^2 - \omega_o^2)^2 + k^2\omega^2} \tag{2.2}$$

Here, f' is the real, first order perturbation of anomalous scattering and is 180° out-of-phase with f_0. The second perturbation term f'' is the imaginary component of radiation and is 90° out-of-phase with f_0. At the absorption edge of an element, the absolute values of these perturbation terms are maximized (Figure 1).

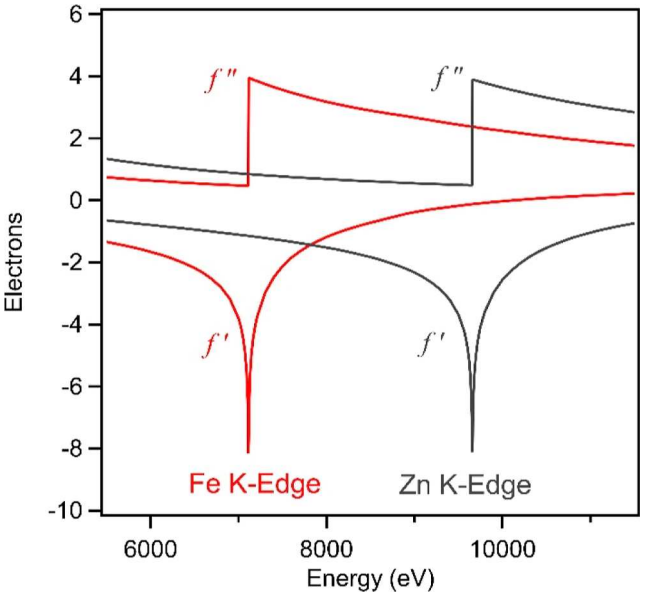

Figure 1. Graphical representation of the theoretical f' and f'' values for Fe^0 and Zn^0, depicted in red and gray, respectively.

In a resonant diffraction experiment on heterometallic clusters, several data sets are collected at energies along the metal K-edges. The anomalous scattering components of each metal site are refined using the diffracted intensities. The anomalous scattering components provide information on metal occupancy because $|f'|$ and $|f''|$ are maximized for the metal whose k-edge is on resonance with the incident K-radiation (Figure 1). A quantitative occupancy value is calculated by decomposing the observed f' values into the contribution from the two different elements using the following equation

$$f'_{obs} = xf'_{M1} + (1 - x)f'_{M2} \tag{3}$$

where f'_{obs} is the measured f' value, f'_{M1} and f'_{M2} are the f' values for a site containing two elements M_1 and M_2, respectively, and x is the relative occupancy of M_1. Consequently, the accuracy of the reference anomalous scattering components for M_1 and M_2 can impact the resolution of occupancy determination. Historically, for materials incorporating two transition metals, relative occupancy has been

https://doi.org/10.1021/jacs.4c10226
J. Am. Chem. Soc. 2024, 146, 30320−30331

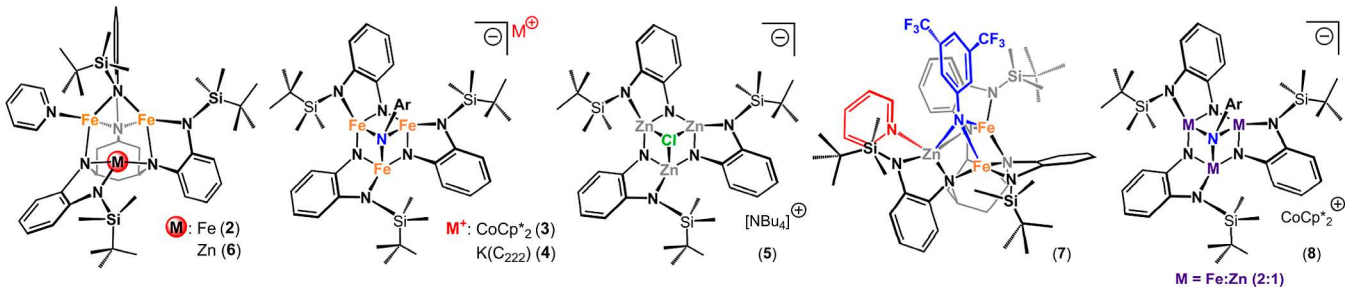

Figure 2. Clusters examined in this study include (^{tbs}L)MFe$_2$(py) (M: Fe, **2**; Zn, **6**); [M$^+$][(^{tbs}L)Fe$_3$(μ^3−NAr)] (Ar = *m*-(CF$_3$)$_2$C$_6$H$_3$), where [M$^+$] = CoCp*$_2$ (**3**) or (2,2,2-crypt)K (**4**); [NBu$_4$][(^{tbs}L)Zn$_3$(μ^3−Cl)] (**5**); (^{tbs}L)Fe$_2$Zn(μ^3−NAr)(py) (**7**); and [CoCp*$_2$][(^{tbs}L)Fe$_2$Zn(μ^3−NAr)] (**8**).

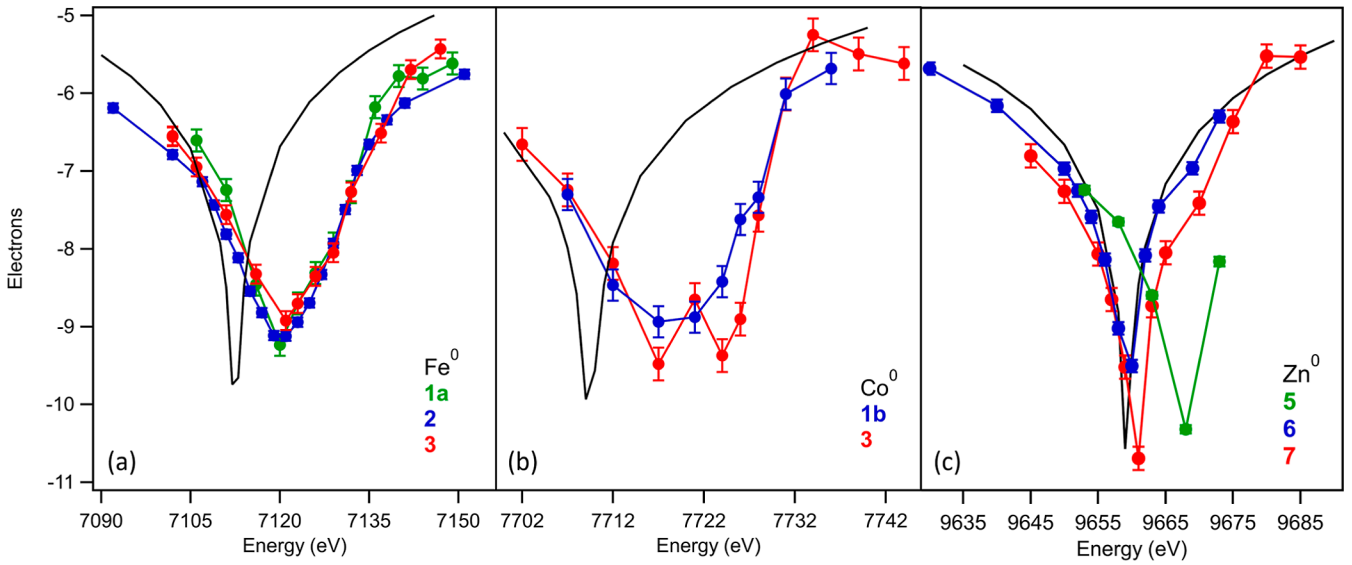

Figure 3. (a) Plot of *f*′ values at the Fe K-edge for Fe ions in FeCp$_2$ (**1a**), (^{tbs}L)Fe$_3$(py) (**2**) (average for all three Fe sites), and [CoCp*$_2$][(^{tbs}L)Fe$_3$(μ^3−NAr)] (**3**) compared against the theoretical Fe^0 curve.[73] (b) Plot of *f*′ values at the Co K-edge for Co ions in CoCp$_2$ (**1b**) and the cobaltocene cation of **3** compared against the theoretical Co^0 curve.[73] (c) Plot of *f*′ values at the Zn K-edge for Zn ion in [NBu$_4$][(^{tbs}L)Zn$_3$(μ^3−Cl)] (**5**), (^{tbs}L)Fe$_2$Zn(py) (**6**), and (^{tbs}L)Fe$_2$Zn(μ^3−NAr)(py) (**7**) compared against the theoretical Zn^0 curve.[73]

determined by comparison of experimental *f*′ and *f*″ values to isostructural, monometallic lattices,[27] derived from theoretical calculations,[28] or compared to *f*′ and *f*″ values for bulk metal samples.[33,35,36] If theoretical values are used in the absence of isostructural, pure metal analogues, systematic error introduction can result if element absorption profiles are heavily influenced by metal coordination environment and oxidation states.[29,37,63,67] As the application of AXD becomes more widespread, we sought to understand the limits of resolution that can be achieved using this diffraction technique.

2.2. Molecular Clusters for AXD and Neutron Studies. We previously reported the preparation of a family of Fe and Zn homonuclear and heteronuclear molecular clusters on the ^{tbs}L (^{tbs}L = 1,3,5-C$_6$H$_9$(NC$_6$H$_4$-*o*-NSiMe$_2$^{t}Bu)$_3$) ligand platform.[5] In the first part of our study, we compare the theoretical anomalous scattering terms for Fe and Zn to that of molecular reference compounds at various wavelengths near the Fe and Zn K-edges. These reference compounds include Cp$_2$Fe (**1a**), Cp$_2$Co (**1b**), and the homotrinuclear complexes (^{tbs}L)Fe$_3$(py) (**2**), [M$^+$][(^{tbs}L)Fe$_3$(μ^3−NAr)] (Ar = *m*-(CF$_3$)$_2$C$_6$H$_3$), where [M$^+$] = CoCp*$_2$ (**3**) or (2,2,2-crypt)K (**4**), and [NBu$_4$]-[(^{tbs}L)Zn$_3$(μ^3−Cl)] (**5**). Complex **4** is isostructural to the previously reported complex **3**, and details of the synthesis can be found in the Supporting Information (S6). We then assessed the error of AXD occupancy studies by calculating the occupancy of each Fe site in **3** at the Fe K-edge using different *f*′ references.

Using the methodology we develop from these studies, we assessed the core site occupancies of [Fe$_2$Zn] clusters: (^{tbs}L)Fe$_2$Zn(py) (**6**), (^{tbs}L)Fe$_2$Zn(μ^3−NAr)(py) (**7**), and [CoCp*$_2$][(^{tbs}L)Fe$_2$Zn(μ^3−NAr)] (**8**). Complex **8** is isostructural to the previously reported cluster [KC$_{222}$][(^{tbs}L)Fe$_2$Zn(μ^3−NAr)]. The large crystal size of **8** allowed for comparison of the AXD occupancy results against that of neutron diffraction. Details on the synthesis and characterization of **8** can be found in the Supporting Information (S6). Details on the synthesis and characterization of all other complexes can be found in our previous publication.[5]

2.3. X-ray Diffraction Data Collection Strategy. X-ray diffraction datasets at energies along the Fe, Co, and Zn K-edges were collected using a synchrotron radiation source at the Advanced Photon Source. Data collection on each crystal began with a full structure determination at 30 keV to assign the position and displacement parameters of each atom. Following the 30 keV full structure collection, an X-ray fluorescence scan across the K-edge(s) of the element(s) of interest was measured. The wavelengths of incident radiation for the AXD studies were selected for each metal K-edge based on the fluorescence scan. Diffraction data was acquired via a series of ϕ scans to obtain roughly 200−2000 unique reflections at each energy. Stable samples were subjected to no more than 12 h of radiation exposure, whereas data collection on more sensitive samples was completed in 8 h or less. X-ray diffraction data was acquired at and near the absorption edge of each transition metal in each sample in increments of 2−10 eV. Data acquired at a second or third absorption edge exhibited greater error, likely due to diminished crystal quality from prolonged radiation exposure. Anomalous scattering components were refined using Jana2020.[74] All theoretical *f*′ and *f*″ values were generated using the XDISP functionality of WinGX (Brennan values).[73]

https://doi.org/10.1021/jacs.4c10226
J. Am. Chem. Soc. 2024, 146, 30320−30331

2.4. Neutron Diffraction Collection Strategy. A large crystal ($0.5 \times 0.6 \times 1.2$ mm^3) of **8** was mounted on a MiTeGen loop with Krytox grease for the neutron diffraction experiment using the SNS TOPAZ single-crystal diffractometer at Oak Ridge National Laboratory. Data were collected at 100 K using the wavelength-resolved time-of-flight (TOF) Laue technique, with neutron wavelengths in the range of 0.65 to 3.4 Å. The diffractometer used for this experiment employs an array of 24 neutron wavelength-resolved 2D area detectors at distances 39.5 to 45.0 cm from the sample. An orientation matrix from initial indexing of the single-crystal sample was imported into the CRYSTALPLAN program[75] to optimize the data collection strategy.

3. RESULTS

3.1. Comparing Theoretical and Experimental *f′* Values. Theoretical f' curves for Fe^0, Co^0, and Zn^0 were compared to experimental curves from Fe, Co, and Zn-containing molecules at their respective K-edges. First, the theoretical Fe^0 f' curve at the Fe K-edge was compared to that for clusters **1a**, **2**, and **3** (Figure 3). The theoretical f' curve for Fe is blue-shifted by approximately 8 eV (measured as the distance between peak minima) from the experimentally determined f' curves (Figure 3a). The f' curves of two Co-containing molecules were compared against the Co^0 f' curve at the Co K-edge. Similarly to the Fe-example, the experimental data are shifted 11 eV higher in energy relative to the theoretical curve. Finally, several zinc-containing samples where the Zn centers remain site-isolated: **5**, **6**, and **7** (the exact occupancies of **6** and **7** will be further discussed in Section 3.4 of this report) were compared against the Zn^0 theoretical curve. Although the theoretical Zn^0 f' curve is not shifted significantly from that of **6** and **7**, it is shifted 9 eV lower in energy from that of **5**.

For Fe, Co, and Zn, the theoretical f' curve is energetically shifted from that of the experimental data. These comparisons indicate that using theoretical f' values as the references for occupancy calculations may introduce systematic error resulting in incorrect calculated values. In many examples of AXD occupancy studies on mixed-metal materials, the theoretical f' value is the only available reference. The synthetic tunability of our trinuclear clusters, however, allows metal atom substitution within the core. This results in structurally analogous homometallic clusters which can then serve as reference compounds for heterometallic clusters (Figure 2). Before utilizing this approach, we wanted to quantify how accurately two isostructural homometallic clusters could reference one another with respect to other reference sources (i.e., theoretical references).[70−72] This study would also provide insight into the intrinsic error of AXD occupancy studies.

3.2. Accuracy of Occupancy Determination. *3.2.1. Establishing the Error Limits of Occupancy Determination Using f′ and f″ Values from Different Sources.* The reduced triiron cluster $[CoCp^*_2][(^{tbs}L)Fe_3(\mu^3{-}NAr)]$ (**3**) was selected to evaluate the accuracy of different f' references for determining site occupancy. While this molecule contains both Fe and Co, exchange between the metal sites is not expected (Figure S7). Therefore, the expectation value for the occupancy of Fe within the trinuclear cluster is 1.0, and the occupancy of Co in the metallocene cation is 1.0.

Deviation of the calculated occupancy from unity provides insight into the overall accuracy of occupancy determination. Additionally, the trinuclear cluster of the anion in **3** is isostructural to that in **4**, and the $CoCp^*_2$ cation of **3** is isostructural to $CoCp_2$ (**1b**). This allows us to assess the similarity of f' values between isostructural molecules.

Occupancy determination at each transition metal substituted site is achieved by considering contributions of each of the potential metal atoms (i.e., Fe, Co) in accordance with eq 3, where f'_{M1} and f'_{M2} are reference values. Prior convention in the application of AXD to site occupancy determination in molecules utilized theorical dispersion correction values $f'_{theoretical}$.[28] Three sources were used to obtain f' dispersion corrections for the occupancy calculations: (1) theoretical values for f'; (2) f' values obtained from related control samples (**4** for Fe, **1b** for Co); and (3) f' values obtained via refinement of **3** in Jana2020, where occupancy of the sites in the trinuclear cluster was constrained to 100% Fe and occupancy of the counterion site was constrained to 100% Co.

The f' values at the Fe K-edge for **3** are depicted graphically in Figure 4. Data from control sample **4** (Fe) was interpolated

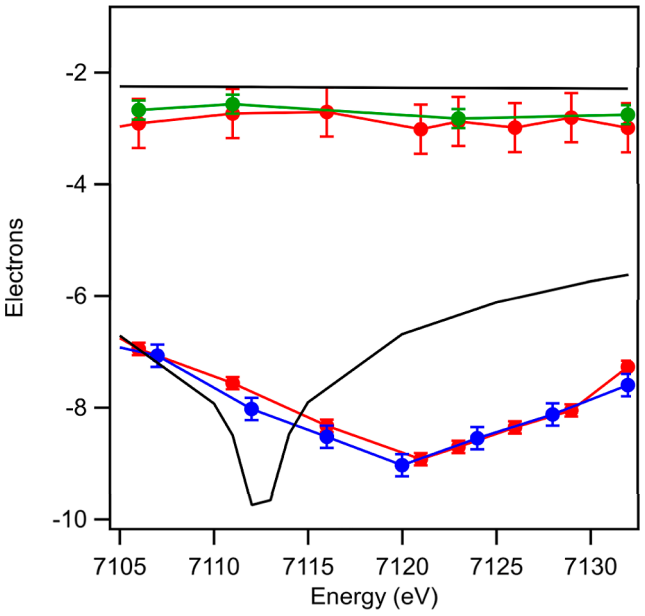

Figure 4. Refined f' values for each Fe site of $[CoCp^*_2][(^{tbs}L)Fe_3(\mu^3{-}NAr)]$ (**3**) (red trace). Black lines represent the theoretical f' values of Fe and Co. Blue and green traces represent f' values obtained from reference compounds $CoCp_2$ (**1b**) (green) and $[(2,2,2\text{-crypt})K]$ $[(^{tbs}L)Fe_3(\mu^3{-}NAr)]$ (**4**) (blue).

using a smoothing function in IgorPro to obtain values between those energies for which diffraction data was collected. The off-edge data from **1b** was fitted using a line function in IgorPro.[76] The red traces represent the f' values obtained from refinement of **3** in Jana2020. Occupancy values were calculated at energies of 7102, 7106, and 7111 eV (Figure 5). These energies were chosen because while near the absorption K-edge of Fe, they are located prior to any pre-edge feature, minimizing effects of coordination number, coordination sphere, and oxidation state on f'. Occupancy of Fe and Co at each of the metal sites was constrained to a sum of 1 overall and simultaneously refined, requiring inputs for f'_{Fe}, and f'_{Co}.

Using theoretical f' reference values resulted in the largest difference in occupancy values from the expected occupancy of 1.0 (Figure 5a). While the theoretical f' does result in an occupancy of 1.0 for Fe in each site of **4** for the first energy (7102 eV), this is untrue for higher energies where the theoretical trace differs substantially from the experimental

https://doi.org/10.1021/jacs.4c10226
J. Am. Chem. Soc. 2024, 146, 30320−30331

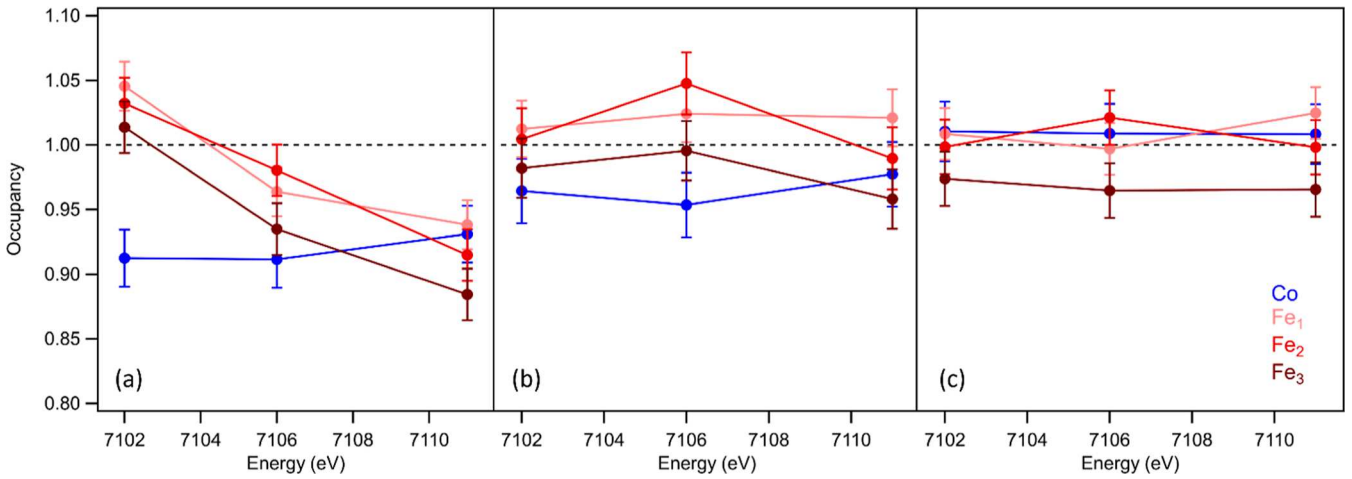

Figure 5. Plots of occupancy values obtained from data collected at 7102, 7106, and 7111 eV for [CoCp*$_2$][(^{tbs}L)Fe$_3$(μ^3−NAr)] (**3**). Calculation of the occupancy of each site was done using f' and f'' values obtained from theoretical curves (a), refinement of data from control samples ($CoCp_2$ (**1b**), [(2,2,2-crypt)K] [(^{tbs}L)Fe$_3$(μ^3−NAr)] (**4**) for Fe) (b), and refinement of the data from **3** in Jana2000 assuming 100% occupancy of the Fe and Co in their respective sites in the crystal structure (c). The series of red traces in each plot represents the refined Fe occupancy of the three different iron sites. The blue trace in each plot represents the refined Co occupancy of the cobalt site. The black dashed line at 1.00 represents the expected occupancy value for each site.

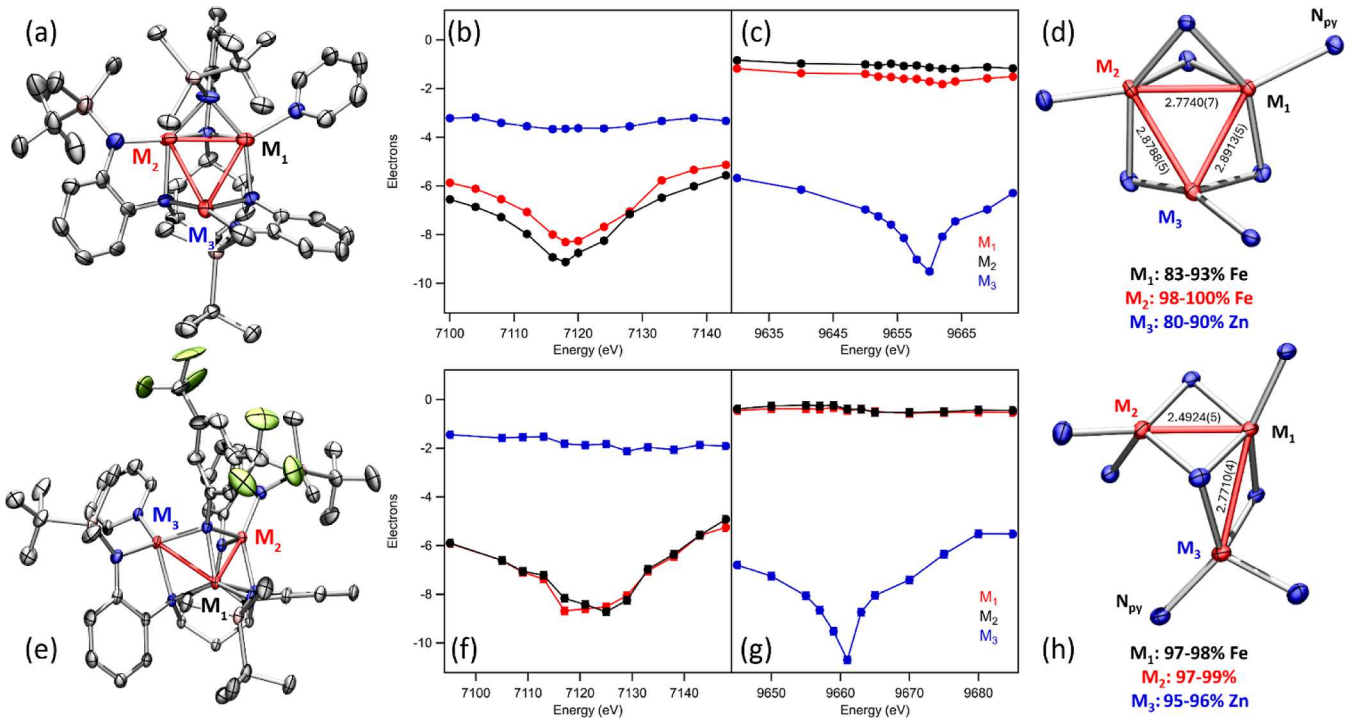

Figure 6. Molecular structures (30 keV) and plots of f' values at the Fe and Zn K-edges and the respective Fe/Zn occupancies at each metal site (^{tbs}L)Fe$_2$Zn(py) (**6**, a−d), and (^{tbs}L)Fe$_2$Zn(μ^3−NAr)(py) (**7**, e−h).

trace. This leads to large discrepancies in the occupancy determinations of the homometallic core. Moreover, the Co site (Figure 5a) is consistently underestimated in occupancy by 8−10% when the theoretical reference f' values are used. Overall, the deviation in occupancy using the theoretical curves is on the order of ±15% within 2σ of the expected occupancy values (Figure 5a).

Using f' and f'' values derived from the structurally analogous triiron and cobaltocene reference complexes (**4** and **1b**), the occupancy calculations yield the anticipated values (Figure 5b). While the reference complex for Co, Cp_2Co^{+2} (**1b**), is in a different oxidation state than the Co^{+3} ion in **3**, the difference in f' values is negligible at the energies selected for occupancy determination. Overall, the deviation in occupancy from the expected value of 1.0 is approximately ±5% or ±10% within 2σ (Figure 5b).

To establish the upper limit of accuracy for occupancy determination, we analyzed the data using f' and f'' values obtained by refinement of **3** in Jana2020[74] where each site was constrained to 100% Fe or Co occupancy. The less-constrained refinement of **3** was compared against these reference f' values. Using this strategy, the deviation of the occupancy determination from unity was further reduced (±4%, ±8%

https://doi.org/10.1021/jacs.4c10226
J. Am. Chem. Soc. 2024, 146, 30320−30331

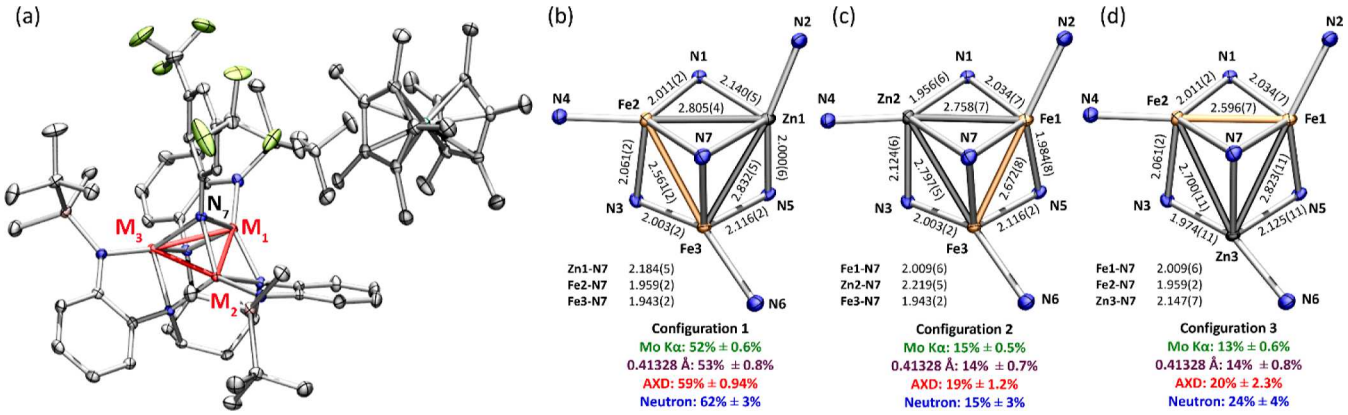

Figure 7. Molecular structure of $[CoCp^*_2][(^{tbs}L)Fe_2Zn(\mu^3{-}NAr)]$ (**8**) (a) (30 keV) and truncated cores showcasing the three orientations (b–d) of the core and their respective occupancies via Mo Kα SCXRD, synchrotron, AXD, and neutron diffraction studies.

with 2σ), but within the error of uncertainty with respect to using the molecular reference compounds (Figure 5c).

Additionally, occupancy values were calculated at the Co K-edge in a similar manner to what as conducted at the Fe K-edge. These studies exhibited much larger errors; ±17% within 2σ for calculations done with theoretical references (Figure S60) and ±14% within 2σ for that done with isostructural references (Figure S61). We attribute this error to the fact that the data at the Co K-edge was collected after the Fe K-edge energies, therefore diminishing the crystal quality due to radiation damage. Moreover, control data was not obtained for **4** at the Co K-edge, and, therefore, theoretical reference values were used in place of experimental ones. For these reasons, the discussion focuses on data collected at the Fe K-edge.

3.3. Applying Occupancy Determination to C_1-Symmetric Mixed Metal Trinuclear Clusters 6 and 7. Refinement of f' values for the metal sites in $(^{tbs}L)Fe_2Zn(py)$ (**6**) and $(^{tbs}L)Fe_2Zn(\mu^3{-}NAr)(py)$ (**7**) in Jana2020[74] yields a perturbation in the f' curves of the two Fe sites at the Fe K-edge (Figure 6b,f) and the f' curve of the Zn site at the Zn K-edge (Figures 6c,g). Conversely the curves for the Zn site at the Fe K-edge and the Fe sites at the Zn K-edge exhibit no perturbation and are essentially flat lines. Thus, the f' data supports the previously assigned conformation of metal substitution within the cores. Calculations of occupancy at each site in **6** and **7** utilizing experimental f' references are described below.

The trinuclear cluster $(^{tbs}L)Fe_2Zn(py)$ (**6**), is isostructural to the analogous triiron cluster $(^{tbs}L)Fe_3(py)$ (**2**). Each metal site in complex **6** has a distinct coordination environment, and as such there may be preferential metal occupancy. The occupancy of Fe and Zn at each metal site was refined at 7100, 7104, 7108 eV. Dispersion correction values for Fe were taken from reference sample **2**, and values for Zn were taken from the Zn site of **7** (see below). Occupancy values were determined as 98–100% Fe at the pyridine bound site (M1, Figure 6d), 83–93% Fe at the nonsolvent bound four-coordinate site (M3, Figure 6d), and 80–90% Zn at the three-coordinate site (M2, Figure 6d). Given that each site falls within 10% error of 100% occupancy, and previously reported Mossbauer data suggests the existence of two distinct Fe sites, all sites were assigned as containing 100% occupancy of either Fe or Zn.

To calculate the site occupancies of $(^{tbs}L)Fe_2Zn(\mu^3{-}NAr)(py)$ (**7**), the occupancy of Fe and Zn at each of the three sites was freely refined using diffraction data collected at energies of 7105 and 7109 eV (just prior to the Fe K-edge). The reference sample selected for determining Fe f' values was the $[(^{tbs}L)Fe_3(\mu^3{-}NAr)]^-$ anion of **3**, which exhibits a similar coordination environment and oxidation state to the cluster core of **7**. No control sample was readily available for the Zn site; thus, the theoretical values were used for the Zn anomalous scattering components at the Fe edge. Given the less pronounced deviation of the experimental f' curves for Zn in **7** from the theoretical curves as compared to Fe or Co, use of the theoretical reference was deemed appropriate especially for energies well below the Zn K-edge. Occupancy at the two Fe sites in **7** was refined to values between 97 and 99% and occupancy at the Zn site was refined to 95–96% as shown in Figure 6h. Given that 1.0 occupancy is within the error of the experiment (established in Section 3.1), all sites were assigned as containing 100% occupancy of either Fe or Zn.

3.4. A Comparison of Methods for Occupancy Determination in a C_3-Symmetric Species with an Unbiased Coordination Environment: $[CoCp^*_2][(^{tbs}L)Fe_2Zn(\mu^3{-}NAr)]$ (8). Reduction of $(^{tbs}L)Fe_2Zn(py)(\mu^3{-}NAr)$ (**7**) with decamethylcobaltocene yields the pseudo-C_3-symmetric imido species $[CoCp^*_2][(^{tbs}L)Fe_2Zn(\mu^3{-}NAr)]$ (**8**), which is structurally analogous to the previously reported $[(2,2,2\text{-crypt})K][(^{tbs}L)Fe_2Zn(\mu^3{-}NAr)]$ cluster. The pyridine bound in **7** has been expelled and the coordination environment at the three metal sites is indistinguishable (Figure 7a). As such, no differences in metal ion coordination sphere bias the metal substitution pattern. While this species is structurally analogous to the related triiron imido $(^{tbs}L)Fe_3(\mu^3{-}NAr)$ (**4**), complex **8** exhibits distinct ^1H and ^{19}F NMR spectra. Furthermore, as we had concluded in our previous publication, no metal-atom redistribution occurs upon reduction of the imido **7**, maintaining the Fe/Zn of 2:1.

Crystallographic studies were performed on the cobalt-reduced cluster **8**, because larger crystals could be obtained than of the analogous complex $[(2,2,2\text{-crypt})K][(^{tbs}L)Fe_2Zn(\mu^3{-}NAr)]$ cluster. Direct comparison of AXD and neutron diffraction was performed on samples produced from the same crystallization. Compound **8** crystallizes in the triclinic space group P1(−), featuring an asymmetric unit comprised of a single trinuclear cluster, countercation, and one molecule of diethyl ether. This structural model provides an added benefit for data collection over $[2,2,2\text{-crypt}(K)][(^{tbs}L)Fe_2Zn(\mu^3{-}NAr)]$, which contained two trinuclear clusters in the

https://doi.org/10.1021/jacs.4c10226
J. Am. Chem. Soc. 2024, 146, 30320–30331

asymmetric unit, and would consequently reduce the data-to-parameter ratio by half in the refinement of f' and f''.[5]

Each metal site of the trinuclear core was modeled with two-part disorder comprised of slightly differing positions for Fe and Zn at each site based on small deviations in M−ligand bond metrics for the two metal ions. Individual metal positions were assigned in reference to M−ligand bond metrics in homometallic species $[NBu_4][(^{tbs}L)Zn_3(\mu^3{-}Cl)]$ (**5**) and $[(2,2,2\text{-crypt})K]$ $[(^{tbs}L)Fe_3(\mu^3{-}NAr)]$ (**4**). The homometallic species provided average $M{-}N_{Si}$ distances of 1.911[2] and 1.947[5] Å for Fe and Zn, respectively; average $M{-}N_{base}$ distances of 1.953[2] and 2.055[2] Å for the two types of basal nitrogen bridges to Zn; and 2.008[5] and 2.070[5] Å for the analogous nitrogen atoms bridging to Fe. The assignment of metal identity based on M−ligand bond metric similarities is also consistent with the shortest M−M contact between the assigned Fe−Fe pairs. A summary of the pertinent bond metrics is presented in Table S28 and the three resulting $[Fe_2Zn]$ configurations are depicted in Figure 7. Free refinement of metal occupancy in each of these conformations using data collected with Mo Kα radiation, suggests an asymmetric incorporation of Zn, where configuration **1** is refined as 52% ± 0.6% of the material, and configurations **2** and **3** are modeled at 15 ± 0.5% and 13% ± 0.6%, respectively. Free refinement of the structural solution collected using synchrotron radiation (λ = 0.41328 Å), yields similar results; 53% ± 0.8% (configuration **1**), 14% ± 0.7% (configuration **2**), and 14% ± 0.8% (configuration **3**).

3.4.1. Occupancy Determination by AXD. For refinement of occupancy by AXD, reference dispersion correction values for Fe and Zn were determined via refinement of diffraction data of homometallic Fe and Zn samples, $[(2,2,2\text{-crypt})K]$ $[(^{tbs}L)Fe_3(\mu^3{-}NAr)]$ (**4**) and $[NBu_4][(^{tbs}L)Zn_3(\mu^3{-}Cl)]$ (**5**), collected at 7100, 7106, 7112, 9653, 9658, and 9663 eV. Using the same structural model as described above, occupancies of the metal sites of the trinuclear core were refined and averaged over the six anomalous data sets to yield the following ratio of the three $[Fe_2Zn]$ configurations: 59% (Std Dev = 0.94%), 19% (Std Dev = 1.2%), and 20% (Std Dev = 2.3%), as depicted in Figure 7.

3.4.2. Occupancy Determination by Neutron Diffraction. The neutron diffraction of $[CoCp^*_2][(^{tbs}L)Fe_2Zn(\mu^3{-}NAr)]$ (**8**) was complicated by the large number of hydrogen atoms of the (^{tbs}L) ligand platform, which limited the intensity of observed reflections due to the high incoherent scattering background from hydrogen. As a result of the weak intensity of the diffraction data, each scan required 10 h to reach the required proton charge, and data could only be collected in 20 different orientations over the course of the available beamtime. Consequently, the data collection strategy was designed to target the reflections predicted to be most sensitive to metal occupancy. X-ray and neutron powder diffraction patterns were simulated using the structural model obtained from Mo Kα radiation to determine which reflections would yield the most information on the metal substitution pattern.

Due to the limited amount of neutron diffraction data obtained, the atomic positions and displacement parameters of all non-hydrogen atoms of the structure were taken from the model refined using the Mo Kα data and fixed in the neutron model. The reflection data obtained from neutron diffraction was used to refine the atomic positions and displacement parameters of the hydrogen atoms and the occupancies of the metal sites using SHELXL-2014 program in ShelXle.[77] The neutron diffraction structure is presented in Figure 8. Refinement of metal occupancies using the neutron data resulted in preferential orientation of the $[Fe_2Zn]$ core: configurations **1**, **2**, and **3** from Figure 7 were refined to 62% ± 3%, 15% ± 3%, and 24% ± 4%, respectively. These values represent the same distribution of Fe and Zn across the three metal sites as determined by anomalous X-ray scattering, within the established ±5% uncertainty (*vide supra*).

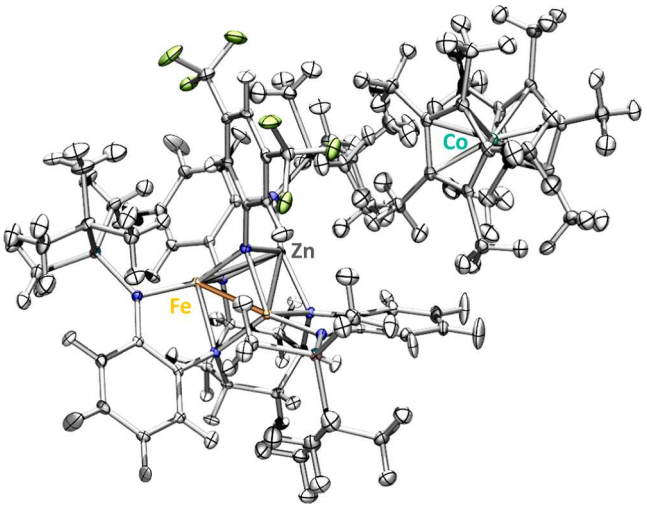

Figure 8. Neutron diffraction crystal structure of $[CoCp^*_2][(^{tbs}L)Fe_2Zn(\mu^3{-}NAr)]$ (**8**), drawn showcasing only configuration **1** at 50% thermal ellipsoid probability (C, gray; H, white; N, blue; Si, pink; F, yellow; Co, aquamarine; Fe, gold; Zn, dark gray). The F_3C disorder and diethyl ether molecule omitted for clarity.

4. DISCUSSION

Given that the conventional application of AXD to molecules has relied on the comparison of experimental f' and f'' values to theoretical values, we first sought to assess their likeness across a variety of metals and metal K-edges. The comparison of theoretical Fe, Co, and Zn f' curves against that of Fe, Co, and Zn-containing molecules (at their respective K-edges) revealed that they are not well correlated. In particular in the case of Fe and Co, the theoretical curves were shifted from experimental by as much as 11 eV.

To understand this discrepancy, we looked toward the theoretical treatment of anomalous scattering. Theoretical f' and f'' values are generated using the XDISP program in WinGX via the following equations

$$\Delta f' = \sum_k \int_{\omega k}^{\infty} \frac{\omega^2 \left(\frac{dg}{d\omega}\right)_k}{\omega_i^2 - \omega^2} d\omega \tag{4}$$

$$\Delta f'' = \frac{1}{2}\pi\omega_i \sum_k \left(\frac{dg}{d\omega}\right)_{k_i} \tag{5}$$

where ω_k is the frequency of the absorption edge, ω_i is the incident frequency, $(dg/d\omega)_k$ is the oscillator density of type k at frequency ω, and $(dg/d\omega)_k d\omega$ is the number of virtual oscillators of type k having frequencies between ω and $\omega + d\omega$.[70−72] The oscillator strength[81] of atoms are determined from self-consistent field relativistic Dirac−Slater wave functions originally employed by Cromer in 1965.[70] This

https://doi.org/10.1021/jacs.4c10226
J. Am. Chem. Soc. 2024, 146, 30320−30331

theoretical model, although incredibly insightful, is solely a function of wavelength, absorption edge, and oscillator strength. The model does not account for the chemical effects on electronic transitions such as oxidation level or covalency. In the case of transition metals, these effects can dominate the features of K-edge X-ray absorption spectra. This is because the energy of the orbitals involved in the pre- and rising-edge transitions, the 3d and 4p orbitals, are heavily influenced by the ligand environment and oxidation level of the metal. This physical description is supported by the large energy shift between the theoretical and experimental f' curves for Fe and Co.

Next, to assess the accuracy of AXD applied to a molecule, we calculated the metal site occupancies of $[CoCp^*_2][(^{tbs}L)Fe_3(\mu^3{-}NAr)]$ (**3**) using the refined f' values for each metal site at the Fe K-edge. Two different f' reference values, theoretical and from an isostructural cluster $[(2,2,2\text{-crypt})K][(^{tbs}L)Fe_3(\mu^3{-}NAr)]$ (**4**), were selected to assess how accurately they yielded the expected results (an occupancy value of 100% Fe at the cluster sites and 100% Co at the cobaltocene site). The calculation using reference values from the isostructural cluster **4** yielded the expected results within ±5% error (±10% with 2σ), whereas the theoretical reference yielded much larger errors (±15% with 2σ). Additionally, by fixing each metal site occupancy to 100% Fe or Co, refining the f' values in Jana2020, and then comparing to the less-constrained f' values, we established the minimum possible error in these studies as 4% (±8% with 2σ). Overall, these studies suggest that use of an isostructural reference compound results in the most accurate calculation of occupancy values. Regardless of the reference f' values used, AXD occupancy studies at minimum have an error of ±10% within 2σ. Corroboration with other spectroscopic methods, such as ^{57}Fe Mössbauer, can help elucidate whether there is metal site mixing in instances where occupancy is within error of unity.

The foregoing studies on occupancy offered valuable insight into how to conduct AXD occupancy studies. As such we suggest the following protocol: (1) acquire a full structure collection at high energy (30 keV) to determine atomic positions and displacement parameters for all subsequent metal K-edge diffraction data sets. This method reduces the number of parameters that require refinement for the low energy diffraction data sets, and therefore minimizes the number of unique reflections that need to be acquired at each K-edge energy. The shortened collection time helps mitigate the decline in data quality resulting from prolonged exposure of the crystal to high flux radiation. (2) Collect X-ray fluorescence scans of the sample to facilitate the selection of energies at which to collect data near the absorption K-edges of the metals in the sample. Incident energies for AXD collection were selected based on the element absorption edge profile. As the element (e.g., Fe, Co, Zn), coordination number, coordination sphere, and oxidation state will impact the K-edge profile, we selected energies prior to the pre-edge feature of the absorption profile for AXD measurements intended for occupancy calculations. In instances where the full K-edge envelope was assessed, diffraction data was acquired at energies across the pre-, rising-, and post-edge regions. (3) Collect diffraction data for structurally similar (when possible) control samples at these energies to determine anomalous scattering components (f' and f'') for each of the metals present in the sample. When structurally similar molecular reference compounds are unavailable, molecular species that best approximate the target metal coordination environment and oxidation state should be used. (4) Finally, collect diffraction data at the same energies for the heterometallic species of interest. Site specific occupancies can then be refined via eq 3 using the data from the heterometallic complexes using the f' and f'' values obtained from the reference samples.

We applied this strategy to three Fe−Zn containing clusters. Applying the AXD method to a C_1-symmetric cluster $(^{tbs}L)Fe_2Zn(py)(\mu^3{-}NAr)$ (**7**) whose spectroscopic analysis suggests no site mixing, we confirmed the identity of the metal sites in **7**, as well as the substitutional homogeneity of the material. Applying the AXD method to C_1-symmetric $(^{tbs}L)ZnFe_2(py)$ (**6**), we corroborated the metal substitution suggested from ^{57}Fe Mössbauer spectroscopy.[5] Lastly, AXD studies were applied to the pseudo-C_3-symmetric $[CoCp^*_2][(^{tbs}L)Fe_2Zn(\mu^3{-}NAr)]$ (**8**) where no bias in coordination environment is present. The results indicate Fe and Zn mix into all three sites. Due to the large crystal size of **8**, we were able to compare the occupancy results of AXD to that of neutron diffraction. The two techniques yield similar metal site occupancies and resolve the dominant core $[Fe_2Zn]$ configurations equally well within error.

As demonstrated in the development of our method for resonant X-ray diffraction, AXD requires the use of suitable reference samples to determine anomalous scattering terms f' and f'' that afford accurate occupancy values for transition metals in molecular heterometallic samples. For materials where no suitable reference complexes are available, AXD referenced to theoretical dispersion correction factors can lead to inaccurate occupancy determinations. In such cases, neutron diffraction, which does not require reference samples, may be the preferred method. However, the significantly longer data collection time required for neutron diffraction, larger requisite crystalline sample size, and nonperiodicity of neutron scattering lengths can limit the utility of the technique. Additionally, analysis of the sample studied herein was complicated by the abundance of hydrogen atoms on the (^{tbs}L) ligand. The high incoherent scattering from the H atoms further lengthened data collection time. Indeed, the data collection strategy employed targeted specific reflections predicted to be most sensitive to metal substitution as a full neutron structure collection could not be obtained in a reasonable time frame. As such, atomic positions and displacement parameters of all non-hydrogen atoms were determined from the Mo Kα data set and only hydrogen atom positions and thermal displacement parameters, and metal occupancies were refined using neutron data. The accuracy of the metal position refinement with Mo Kα diffraction data is due to the appreciable difference in scattering amplitudes between Zn and Fe at that wavelength (15% difference when calculated assuming f_0 is equal to the number of electrons in the atom).

5. CONCLUSION

The foregoing work describes the application of AXD and neutron diffraction to the determination of metal occupancy in molecular species containing two first row transition metals. In our efforts to develop a method for AXD, we established that the use of theoretical anomalous scattering values in occupancy determination per convention leads to large errors in calculated occupancy values. Substitution of the theoretical f' and f'' values with experimentally derived terms from molecular control samples minimizes error and provides a ±5%

https://doi.org/10.1021/jacs.4c10226
J. Am. Chem. Soc. 2024, 146, 30320−30331

resolution for occupancy values obtained. The prescribed method was applied to a family of heterometallic clusters, and the site-specific elemental analysis was performed to reveal overall compositional analysis. This work has established a standardized protocol for implementing AXD and can be used as a benchmark for evaluating the accuracy of this technique as applied to molecular species. Additionally, the application of both AXD and neutron diffraction to a [Fe_2Zn] imido cluster to identify site-specific metal substitution and occupancy yielded comparable results and suggest the utility of either technique for occupancy determination. Comparison of the neutron data to that obtained by AXD establishes the accuracy of AXD for determination of metal occupancy in heterometallic molecular clusters. Moreover, this work advances previous implementation of neutron diffraction on molecular species, as the only other reported application of neutron diffraction to a heterometallic molecular species analyzed materials with no site mixing.[69] This work shows that limitations to accurate occupancy calculations in heterometallic materials depend on whether appropriate homometallic references are available or synthetically accessible. In light of this limitation, future work will look at bench marking the accuracy of occupancy calculations as a function of energetic distance from the absolute metal K-edge, as we suspect that theoretically generated f' values become more physically accurate as the incident radiation is red-shifted from the absolute K-edge.

■ ASSOCIATED CONTENT

Supporting Information

The Supporting Information is available free of charge at https://pubs.acs.org/doi/10.1021/jacs.4c10226.

Materials and methods; synthesis and characterization; crystallographic data (PDF)

Accession Codes

CCDC 2360330 and 2360857−2360863 contain the supplementary crystallographic data for this paper. These data can be obtained free of charge via www.ccdc.cam.ac.uk/data_request/cif, or by emailing data_request@ccdc.cam.ac.uk, or by contacting The Cambridge Crystallographic Data Centre, 12 Union Road, Cambridge CB2 1EZ, UK; fax: +44 1223 336033.

■ AUTHOR INFORMATION

Corresponding Author

Theodore A. Betley − *Department of Chemistry and Chemical Biology, Harvard University, Cambridge, Massachusetts 02138, United States;* orcid.org/0000-0001-5946-9629; Email: betley@chemistry.harvard.edu

Authors

Cristin E. Juda − *Department of Chemistry and Chemical Biology, Harvard University, Cambridge, Massachusetts 02138, United States*

Claire E. Casaday − *Department of Chemistry and Chemical Biology, Harvard University, Cambridge, Massachusetts 02138, United States;* orcid.org/0000-0002-9238-0463

Justin J. Teesdale − *Department of Chemistry and Chemical Biology, Harvard University, Cambridge, Massachusetts 02138, United States*

Amymarie K. Bartholomew − *Department of Chemistry and Chemical Biology, Harvard University, Cambridge, Massachusetts 02138, United States;* orcid.org/0000-0002-2092-1718

Benjamin Lin − *Department of Chemistry and Chemical Biology, Harvard University, Cambridge, Massachusetts 02138, United States*

Kurtis M. Carsch − *Department of Chemistry and Chemical Biology, Harvard University, Cambridge, Massachusetts 02138, United States;* orcid.org/0000-0003-4432-7518

Rebecca A. Musgrave − *Department of Chemistry and Chemical Biology, Harvard University, Cambridge, Massachusetts 02138, United States;* orcid.org/0000-0001-9404-0422

Shao-Liang Zheng − *Department of Chemistry and Chemical Biology, Harvard University, Cambridge, Massachusetts 02138, United States;* orcid.org/0000-0002-6432-9943

Xiaoping Wang − *Oak Ridge National Laboratory, Oak Ridge, Tennessee 37830, United States;* orcid.org/0000-0001-7143-8112

Christina M. Hoffmann − *Oak Ridge National Laboratory, Oak Ridge, Tennessee 37830, United States*

SuYin Wang − *NSF's ChemMatCARS, The University of Chicago, Lemont, Illinois 60429, United States;* orcid.org/0000-0001-8474-9817

Yu Sheng Chen − *NSF's ChemMatCARS, The University of Chicago, Lemont, Illinois 60429, United States*

Complete contact information is available at: https://pubs.acs.org/10.1021/jacs.4c10226

Notes

The authors declare no competing financial interest.

■ ACKNOWLEDGMENTS

C.E.J., C.E.C., and K.M.C. thank the NSF for Predoctoral Fellowships. K.M.C. acknowledges the Fannie & John Hertz Foundation for a predoctoral fellowship. A.K.B. is grateful for support from a Smith Family Graduate Science and Engineering Fellowship. R.A.M. gratefully acknowledges postdoctoral support from the European Union's Horizon 2020 Research and Innovation Programme under grant agreement no. 752684. T.A.B. acknowledges support through grants from the NIH (GM-098395), DOE (DE-SC0008313), NSF (CHE-2247817), and Harvard University. We thank the support from the X-ray core facility at Harvard University of the Major Research Instrumentation (MRI) Program of the National Science Foundation (NSF) under Award Numbers 2216066. Crystallographic data for 1 and 3 were obtained at ChemMatCARS Sector 15 at the Advanced Photon Source (APS). APS is a U.S. Department of Energy (DOE) Office of Science User Facility operated for the DOE Office of Science by Argonne National Laboratory under Contract no. DE-AC02-06CH11357. ChemMatCARS Sector 15 is supported by the National Science Foundation under grant number NSF/CHE-1834750. This research used resources at the Spallation Neutron Source, a DOE Office of Science User Facility operated by the Oak Ridge National Laboratory. The beam time was allocated to BL012, the TOPAZ single crystal TOF Laue diffractometer on proposal number IPTS-19168.1. This work was adapted in part from the thesis work submitted by C.E.J., Harvard University.

■ ABBREVIATION

AXD, anomalous X-ray dispersion/diffraction.

REFERENCES

(1) Ertl, G.; Prigge, D.; Schloegl, R.; Weiss, M. Surface characterization of ammonia synthesis catalysts. *J. Catal.* **1983**, *79* (2), 359−377.

(2) Dobbek, H.; Svetlitchnyi, V.; Gremer, L.; Huber, R.; Meyer, O. Crystal Structure of a Carbon Monoxide Dehydrogenase Reveals a [Ni-4Fe-5S] Cluster. *Science* **2001**, *293* (5533), 1281−1285.

(3) Dobbek, H.; Gremer, L.; Kiefersauer, R.; Huber, R.; Meyer, O. Catalysis at a dinuclear [CuSMo(O)OH] cluster in a CO dehydrogenase resolved at 1.1-Å resolution. *Proc. Natl. Acad. Sci. U.S.A.* **2002**, *99* (25), 15971−15976.

(4) Younker, J. M.; Krest, C. M.; Jiang, W.; Krebs, C.; Bollinger, J. M., Jr.; Green, M. T. Structural Analysis of the Mn(IV)/Fe(III) Cofactor of Chlamydia trachomatis Ribonucleotide Reductase by Extended X-ray Absorption Fine Structure Spectroscopy and Density Functional Theory Calculations. *J. Am. Chem. Soc.* **2008**, *130* (45), 15022−15027.

(5) Juda, C. E.; Handford, R. C.; Bartholomew, A. K.; Powers, T. M.; Gu, N. X.; Meyer, E.; Roth, N.; Chen, Y.-S.; Zheng, S.-L.; Betley, T. A. Cluster dynamics of heterometallic trinuclear clusters during ligand substitution, redox chemistry, and group transfer processes. *Chem. Sci.* **2024**, *15*, 8242−8248.

(6) Thompson, N. B.; Namkoong, G.; Skeel, B. A.; Suess, D. L. M. Facile and Dynamic Cleavage of Every Iron−Sulfide Bond in Cuboidal Iron−Sulfur Clusters. *Proc. Natl. Acad. Sci. U.S.A.* **2023**, *120*, No. e2210528120.

(7) Badding, E. D.; Srisantitham, S.; Lukoyanov, D. A.; Hoffman, B. M.; Suess, D. L. M. Connecting the Geometric and Electronic Structures of The Nitrogenase Iron−Molybdenum Cofactor through Site-Selective ^{57}Fe Labelling. *Nat. Chem.* **2023**, *15*, 658−665.

(8) Namkoong, G.; Suess, D. L. M. Cluster-selective ^{57}Fe Labeling of a Twitch-Domain-Containing Radical SAM Enzyme. *Chem. Sci.* **2023**, *14*, 7492−7499.

(9) Nguyen, A. I.; Suess, D. L. M.; Darago, L. E.; Oyala, P. H.; Levine, D. S.; Ziegler, M. S.; Britt, R. D.; Tilley, T. D. Manganese−Cobalt Oxido Cubanes Relevant to Manganese-Doped Water Oxidation Catalysts. *J. Am. Chem. Soc.* **2017**, *139*, 5579−5587.

(10) Zhang, J.; Wu, Z.; Polo-Garzon, F. Recent Developments in Revealing the Impact of Complex Metal Oxide Reconstruction on Catalysis. *ACS Catal.* **2023**, *13*, 15393−15403.

(11) Wheeler, T. A.; Tilley, T. D. Metal−Metal Redox Exchange to Produce Heterometallic Manganese−Cobalt Oxo Cubanes via a "Dangler" Intermediate. *J. Am. Chem. Soc.* **2024**, *146* (29), 20279−20290.

(12) James, R. W. *Optical Principles of the Diffraction of X-rays*; Ox Bow Pr, 1954.

(13) Waseda, Y. *Anomalous X-Ray Scattering for Materials Characterization*; Springer, 2002.

(14) Hammond, C. *The Basics of Crystallography and Diffraction*; Oxford University Press, 1997.

(15) Helliwell, J. R.; Helliwell, M.; Kaucic, V.; Logar, N. Z. Resonant elastic X-ray scattering in chemistry and materials science. *Eur. Phys. J. Spec. Top.* **2012**, *208* (1), 245−257.

(16) Garino, C.; Borfecchia, E.; Gobetto, R.; van Bokhoven, J. A.; Lamberti, C. Determination of the electronic and structural configuration of coordination compounds by synchrotron-radiation techniques. *Coord. Chem. Rev.* **2014**, *277*−*278*, 130−186.

(17) Meurer, F.; Dolomanov, O. V.; Hennig, C.; Peyerimhoff, N.; Kleemiss, F.; Puschmann, H.; Bodensteiner, M. Refinement of anomalous dispersion correction parameters in single-crystal structure determinations. *IUCrJ.* **2022**, *9* (5), 604−609.

(18) Hendrickson, W. A. Determination of Macromolecular Structures from Anomalous Diffraction of Synchrotron Radiation. *Science* **1991**, *254* (5028), 51−58.

(19) Goldman, P. J.; Grove, T. L.; Sites, L. A.; McLaughlin, M. I.; Booker, S. J.; Drennan, C. L. X-ray structure of an AdoMet radical activase reveals an anaerobic solution for formylglycine posttranslational modification. *Proc. Natl. Acad. Sci. U.S.A.* **2013**, *110* (21), 8519−8524.

(20) Dowling, D. P.; Bruender, N. A.; Young, A. P.; McCarty, R. M.; Bandarian, V.; Drennan, C. L. Radical SAM enzyme QueE defines a new minimal core fold and metal-dependent mechanism. *Nat. Chem. Biol.* **2014**, *10* (2), 106−112.

(21) Hendrickson, W. A. Anomalous diffraction in crystallographic phase evaluation. *Q. Rev. Biophys.* **2014**, *47* (1), 49−93.

(22) Bowman, S. E. J.; Bridwell-Rabb, J.; Drennan, C. L. Metalloprotein Crystallography: More than a Structure. *Acc. Chem. Res.* **2016**, *49* (4), 695−702.

(23) Liu, Q.; Hendrickson, W. A. Contemporary Use of Anomalous Diffraction in Biomolecular Structure Analysis. In *Protein Crystallography: Methods and Protocols*; Springer: New York, 2017; pp 377−399.

(24) Griese, J. J.; Högbom, M. Location-specific quantification of protein-bound metal ions by X-ray anomalous dispersion: Q-XAD. *Acta Cryst. D* **2019**, *75* (8), 764−771.

(25) Bradley, A. J.; Rodgers, J. W.; Bragg, W. L. The crystal structure of the heusler alloys. *Proc. R. Soc. Lon. Ser. A Contain. Pap. Math. Phys. Character* **1934**, *144* (852), 340−359.

(26) Dickins, G. J.; Douglas, A. M. B.; Taylor, W. H. The crystal structure of the Co−Cr σ phase. *Acta Crystallogr.* **1956**, *9* (3), 297−303.

(27) Yakel, H. L. Determination of the cation site-occupation parameter in a cobalt ferrite from Synchrotron-Radiation diffraction data. *J. Phys. Chem. Solids* **1980**, *41* (10), 1097−1104.

(28) Yakel, H. Atom distributions in sigma phases. I. Fe and Cr atom distributions in a binary sigma phase equilibrated at 1063, 1013 and 923 K. *Acta Crystallogr., Sect. B* **1983**, *39* (1), 20−28.

(29) Wulf, R. Experimental distinction of elements with similar atomic number using anomalous dispersion (δ synthesis): an application of synchrotron radiation in crystal structure analysis. *Acta Crystallogr., Sect. A* **1990**, *46* (8), 681−688.

(30) Wilkinson, A. P.; Cox, D. E.; Cheetham, A. K. Some aspects of the collection and analysis of powder diffraction data near X-ray absorption edges; resonant diffraction studies of the garnets $Y_3Fe_5O_{12}$ and $Y_3Ga_5O_{12}$. *J. Phys. Chem. Solids* **1991**, *52* (10), 1257−1266.

(31) Ismunandar; Hunter, B. A.; Kennedy, B. J. Cation disorder in the ferroelectric Aurivillius phase $PbBi_2Nb_2O_9$: an anamolous dispersion X-ray diffraction study. *Solid State Ionics* **1998**, *112* (3), 281−289.

(32) Wilkinson, A. P.; Lind, C.; Young, R. A.; Shastri, S. D.; Lee, P. L.; Nolas, G. S. Preparation, Transport Properties, and Structure Analysis by Resonant X-ray Scattering of the Type I Clathrate $Cs_8Cd_4Sn_{42}$. *Chem. Mater.* **2002**, *14* (3), 1300−1305.

(33) Zhang, Y.; Wilkinson, A. P.; Nolas, G. S.; Lee, P. L.; Hodges, J. P. Strategies for solving neighboring-element problems: a case study using resonant X-ray diffraction and pulsed neutron diffraction to examine $Sr_8Ga_{16}Ge_{30}$. *J. Appl. Crystallogr.* **2003**, *36* (5), 1182−1189.

(34) Zhang, Y.; Wilkinson, A. P.; Lee, P. L.; Shastri, S. D.; Shu, D.; Chung, D. Y.; Kanatzidis, M. G. Determining metal ion distributions using resonant scattering at very high-energy K-edges: Bi/Pb in $Pb_5Bi_6Se_{14}$. *J. Appl. Crystallogr.* **2005**, *38* (3), 433−441.

(35) Freedman, D. E.; Han, T. H.; Prodi, A.; Müller, P.; Huang, Q.-Z.; Chen, Y.-S.; Webb, S. M.; Lee, Y. S.; McQueen, T. M.; Nocera, D. G. Site Specific X-ray Anomalous Dispersion of the Geometrically Frustrated Kagomé Magnet, Herbertsmithite, $ZnCu_3(OH)_6C_{l2}$. *J. Am. Chem. Soc.* **2010**, *132* (45), 16185−16190.

(36) Helliwell, M.; Helliwell, J. R.; Kaucic, V.; Zabukovec Logar, N.; Teat, S. J.; Warren, J. E.; Dodson, E. J. Determination of zinc incorporation in the Zn-substituted gallophosphate ZnULM-5 by multiple wavelength anomalous dispersion techniques. *Acta Crystallogr., Sect. B* **2010**, *66* (3), 345−357.

(37) Brozek, C. K.; Cozzolino, A. F.; Teat, S. J.; Chen, Y.-S.; Dincă, M. Quantification of Site-Specific Cation Exchange in Metal−Organic Frameworks Using Multi-Wavelength Anomalous X-ray Dispersion. *Chem. Mater.* **2013**, *25* (15), 2998−3002.

(38) Powers, T. M.; Gu, N. X.; Fout, A. R.; Baldwin, A. M.; Hernández Sánchez, R.; Alfonso, D. M.; Chen, Y.-S.; Zheng, S.-L.;

https://doi.org/10.1021/jacs.4c10226
J. Am. Chem. Soc. 2024, 146, 30320−30331

Betley, T. A. Synthesis of Open-Shell, Bimetallic Mn/Fe Trinuclear Clusters. *J. Am. Chem. Soc.* **2013**, *135* (38), 14448−14458.
(39) Zall, C. M.; Clouston, L. J.; Young, V. G., Jr.; Ding, K.; Kim, H. J.; Zherebetskyy, D.; Chen, Y.-S.; Bill, E.; Gagliardi, L.; Lu, C. C. Mixed-Valent Dicobalt and Iron−Cobalt Complexes with High-Spin Configurations and Short Metal−Metal Bonds. *Inorg. Chem.* **2013**, *52* (16), 9216−9228.
(40) Zhang, L.; Kaiser, J. T.; Meloni, G.; Yang, K.-Y.; Spatzal, T.; Andrade, S. L. A.; Einsle, O.; Howard, J. B.; Rees, D. C. The Sixteenth Iron in the Nitrogenase MoFe Protein. *Angew. Chem., Int. Ed.* **2013**, *52* (40), 10529−10532.
(41) Eisenhart, R. J.; Carlson, R. K.; Clouston, L. J.; Young, V. G., Jr.; Chen, Y.-S.; Bill, E.; Gagliardi, L.; Lu, C. C. Influence of Copper Oxidation State on the Bonding and Electronic Structure of Cobalt−Copper Complexes. *Inorg. Chem.* **2015**, *54* (23), 11330−11338.
(42) Miller, D. L.; Siedschlag, R. B.; Clouston, L. J.; Young, V. G., Jr.; Chen, Y.-S.; Bill, E.; Gagliardi, L.; Lu, C. C. Redox Pairs of Diiron and Iron−Cobalt Complexes with High-Spin Ground States. *Inorg. Chem.* **2016**, *55* (19), 9725−9735.
(43) Poptic, A. L.; Chen, Y.-P.; Chang, T.; Chen, Y.-S.; Moore, C. E.; Zhang, S. Site-Differentiated $Mn^{II}Fe^{II}$ Complex Reproducing the Selective Assembly of Biological Heterobimetallic Mn/Fe Cofactors. *J. Am. Chem. Soc.* **2023**, *145* (6), 3491−3498.
(44) Guss, J. M.; Merritt, E. A.; Phizackerley, R. P.; Hedman, B.; Murata, M.; Hodgson, K. O.; Freeman, H. C. Phase Determination by Multiple-Wavelength X-Ray Diffraction: Crystal Structure of a Basic "Blue" Copper Protein from Cucumbers. *Science* **1988**, *241* (4867), 806−811.
(45) Alayoglu, P.; Chang, T.; Yan, C.; Chen, Y.-S.; Mankad, N. P. Uncovering a CF_3 Effect on X-ray Absorption Energies of $[Cu(CF_3)_4]^-$ and Related Copper Compounds by Using Resonant Diffraction Anomalous Fine Structure (DAFS) Measurements. *Angew. Chem., Int. Ed.* **2023**, *135* (51), No. e202313744.
(46) Gao, Y.; Frost-Jensen, A.; Pressprich, M. R.; Coppens, P.; Marquez, A.; Dupuis, M. Valence contrast by synchrotron resonance scattering: application to a mixed-valence manganese compound. *J. Am. Chem. Soc.* **1992**, *114* (23), 9214−9215.
(47) Gao, Y.; Pressprich, M. R.; Coppens, P. Anamalous-scattering contrast study of the mixed-valence charge-density-wave conductor $NbSe_3$. *Acta Crystallogr., Sect. A* **1993**, *49* (1), 216−219.
(48) Wu, G.; Zhang, Y.; Ribaud, L.; Coppens, P.; Wilson, C.; Iversen, B. B.; Larsen, F. K. Multitemperature Resonance-Diffraction and Structural Study of the Mixed-Valence Complex $[Fe_3O(OOCC(CH_3)_3)_6(C_5H_5N)_3]$. *Inorg. Chem.* **1998**, *37* (23), 6078−6083.
(49) Einsle, O.; Andrade, S. L. A.; Dobbek, H.; Meyer, J.; Rees, D. C. Assignment of Individual Metal Redox States in a Metalloprotein by Crystallographic Refinement at Multiple X-ray Wavelengths. *J. Am. Chem. Soc.* **2007**, *129* (8), 2210−2211.
(50) Spatzal, T.; Schlesier, J.; Burger, E.-M.; Sippel, D.; Zhang, L.; Andrade, S. L. A.; Rees, D. C.; Einsle, O. Nitrogenase FeMoco investigated by spatially resolved anomalous dispersion refinement. *Nat. Commun.* **2016**, *7* (1), 10902.
(51) Hernández Sánchez, R.; Champsaur, A. M.; Choi, B.; Wang, S. G.; Bu, W.; Roy, X.; Chen, Y.-S.; Steigerwald, M. L.; Nuckolls, C.; Paley, D. W. Electron Cartography in Clusters. *Angew. Chem., Int. Ed.* **2018**, *57* (42), 13815−13820.
(52) Arnett, C. H.; Kaiser, J. T.; Agapie, T. Remote Ligand Modifications Tune Electronic Distribution and Reactivity in Site-Differentiated, High-Spin Iron Clusters: Flipping Scaling Relationships. *Inorg. Chem.* **2019**, *58* (23), 15971−15982.
(53) Bartholomew, A. K.; Teesdale, J. J.; Hernández Sánchez, R.; Malbrecht, B. J.; Juda, C. E.; Ménard, G.; Bu, W.; Iovan, D. A.; Mikhailine, A. A.; Zheng, S.-L.; Sarangi, R.; Wang, S. G.; Chen, Y.-S.; Betley, T. A. Exposing the inadequacy of redox formalisms by resolving redox inequivalence within isovalent clusters. *Proc. Natl. Acad. Sci. U.S.A.* **2019**, *116* (32), 15836−15841.
(54) Bartholomew, A. K.; Musgrave, R. A.; Anderton, K. J.; Juda, C. E.; Dong, Y.; Bu, W.; Wang, S.-Y.; Chen, Y.-S.; Betley, T. A. Revealing redox isomerism in trichromium imides by anomalous diffraction. *Chem. Sci.* **2021**, *12* (47), 15739−15749.
(55) Lennartz, F.; Jeoung, J.-H.; Ruenger, S.; Dobbek, H.; Weiss, M. S. Determining the oxidation state of elements by X-ray crystallography. *Acta Cryst. D* **2022**, *78* (2), 238−247.
(56) Alayoglu, P.; Chang, T.; Lorenzo Ocampo, M. V.; Murray, L. J.; Chen, Y.-S.; Mankad, N. P. Metal Site-Specific Electrostatic Field Effects on a Tricopper(I) Cluster Probed by Resonant Diffraction Anomalous Fine Structure (DAFS). *Inorg. Chem.* **2023**, *62* (37), 15267−15276.
(57) Bacon, G. *X-Ray and Neutron Diffraction*; Pergamon Press, 1966.
(58) Sears, V. F. Neutron scattering lengths and cross sections. *Neutron News* **1992**, *3* (3), 26−37.
(59) Williams, A.; Kwei, G. H.; Ortiz, A. T.; Karnowski, M.; Warburton, W. K. Combined neutron and x-ray powder diffraction study of Fe0.50Co0.48V0.02. *J. Mater. Res.* **1990**, *5* (6), 1197−1200.
(60) Sinclair, D. C.; Aranda, M. A. G.; Attfield, P.; Rodríguez-Carvajal, J. Cation distribution and composition of the Tl-2223 superconductor from combined powder neutron and resonant X-ray diffraction. *Physica C* **1994**, *225* (3−4), 307−316.
(61) Pramanick, A.; Wang, X. P.; An, K.; Stoica, A. D.; Yi, J.; Gai, Z.; Hoffmann, C.; Wang, X. L. Structural modulations and magnetic properties of off-stoichiometric Ni-Mn-Ga magnetic shape memory alloys. *Phys. Rev. B* **2012**, *85* (14), 144412.
(62) Battle, P. D.; Blundell, S. J.; Coldea, A. I.; Cussen, E. J.; Rosseinsky, M. J.; Singleton, J.; Spring, L. E.; Vente, J. F. Crystal structure and electronic properties of $Ca_4Mn_2TiO_{9.93}$, an n = 3 Ruddlesden-Popper compound. *J. Mater. Chem.* **2001**, *11* (1), 160−167.
(63) Warner, J. K.; Wilkinson, A. P.; Cheetham, A. K.; Cox, D. E. Comparative study of elemental contrast by resonant x-ray and neutron powder diffraction. *J. Phys. Chem. Solids* **1991**, *52* (10), 1251−1256.
(64) Lehmann, S.; Marrón, D. F.; León, M.; Feyerherm, R.; Dudzik, E.; Friedrich, E. J.; Tovar, M.; Tomm, Y.; Wolf, C.; Schorr, S.; Schedel-Niedrig, T.; Lux-Steiner, M. C.; Merino, J. M. Long-range structure of $Cu(In_xGa_{1-x})_3Se_5$: A complementary neutron and anomalous x-ray diffraction study. *J. Appl. Phys.* **2011**, *109* (1), 013518.
(65) Whittle, K. R.; Hyatt, N. C.; Smith, K. L.; Margiolaki, I.; Berry, F. J.; Knight, K. S.; Lumpkin, G. R. Combined neutron and X-ray diffraction determination of disorder in doped zirconolite-2M. *Am. Mineral.* **2012**, *97* (2−3), 291−298.
(66) Christensen, M.; Lock, N.; Overgaard, J.; Iversen, B. B. Crystal Structures of Thermoelectric n- and p-type $Ba_8Ga_{16}Ge_{30}$ Studied by Single Crystal, Multitemperature, Neutron Diffraction, Conventional X-ray Diffraction and Resonant Synchrotron X-ray Diffraction. *J. Am. Chem. Soc.* **2006**, *128* (49), 15657−15665.
(67) Sibille, R.; Mazet, T.; Malaman, B.; Wang, Q.; Didelot, E.; François, M. Site-Dependent Substitutions in Mixed-Metal Metal−Organic Frameworks: A Case Study and Guidelines for Analogous Systems. *Chem. Mater.* **2015**, *27* (1), 133−140.
(68) Coppens, P. Comparative X-Ray and Neutron Diffraction Study of Bonding Effects in *s*-Triazine. *Science* **1967**, *158* (3808), 1577−1579.
(69) Lieberman, C. M.; Barry, M. C.; Wei, Z.; Rogachev, A. Y.; Wang, X.; Liu, J.-L.; Clérac, R.; Chen, Y.-S.; Filatov, A. S.; Dikarev, E. V. Position Assignment and Oxidation State Recognition of Fe and Co Centers in Heterometallic Mixed-Valent Molecular Precursors for the Low-Temperature Preparation of Target Spinel Oxide Materials. *Inorg. Chem.* **2017**, *56* (16), 9574−9584.
(70) Cromer, D. Anomalous dispersion corrections computed from self-consistent field relativistic Dirac-Slater wave functions. *Acta Crystallogr.* **1965**, *18* (1), 17−23.
(71) Cromer, D. T.; Liberman, D. Relativistic Calculation of Anomalous Scattering Factors for X Rays. *J. Chem. Phys.* **1970**, *53* (5), 1891−1898.

https://doi.org/10.1021/jacs.4c10226
J. Am. Chem. Soc. 2024, 146, 30320−30331

(72) Cromer, D. T. Calculation of anomalous scattering factors at arbitrary wavelengths. *J. Appl. Crystallogr.* **1983**, *16* (4), 437.
(73) Farrugia, L. J. WinGX suite for small-molecule single-crystal crystallography. *J. Appl. Crystallogr.* **1999**, *32* (4), 837−838.
(74) Petricek, V.; Palatinus, L.; Plasil, J.; Dusek, M. *JANA2020. Institute of Physics*; Czech Academy of Sciences: Prague, Czech Republic, 2023.
(75) Zikovsky, J.; Peterson, P. F.; Wang, X. P.; Frost, M.; Hoffmann, C. CrystalPlan: An Experiment-planning Tool for Crystallography. *J. Appl. Crystallogr.* **2011**, *44*, 418−423.
(76) Igor Pro, WaveMetrics, Lake Oswego, OR, USA.
(77) Sheldrick, G. M. A short history of SHELX. *Acta Crystallogr., Sect. A* **2008**, *64*, 112−122.
(78) Meurer, F.; Morrison, G.; Hischa, B.; zur Loye, H.-C.; Hennig, C.; Bodensteiner, M. Improvement of Single-Crystal Structures of Very Heavy Element Compounds by Refining Anomalous Dispersion Parameters. *Inorg. Chem.* **2024**, *63* (34), 15784−15790.
(79) Leinders, G.; Grendal, O. G.; Arts, I.; Bes, R.; Prozheev, I.; Orlat, S.; Fitch, A.; Kvashnina, K.; Verwerft, M. Refinement of the uranium dispersion corrections from anomalous diffraction. *J. Appl. Crystallogr.* **2024**, *57* (2), 284−295.
(80) Wieser, J.; Wardecki, D.; Fischer, J. W. A.; Newton, M. A.; Dejoie, C.; Knorpp, A. J.; Jeschke, G.; Rzepka, P.; van Bokhoven, J. A. Quantifying the Hydration-Dependent Dynamics of Copper Migration and Activity in Zeolite Omega for the Partial Oxidation of Methane. *Angew. Chem. Intl.* **2024**, No. e202407395.
(81) The oscillator strength is a dimensionless quantity that describes the probability of photoelectric absorption or emission of electromagnetic radiation as electrons within atoms or molecules transition between different energetic states. Ref 12.

https://doi.org/10.1021/jacs.4c10226
J. Am. Chem. Soc. 2024, 146, 30320−30331